PREDICTIONS OF AVERAGE SILICA PARTICLE SIZE OVER TIME UNDER GEOTHERMAL CONDITIONS

Shuying Chen[1], Kevin Brown[2], and Mark Jermy[1]

[1] Department of Mechanical Engineering, University of Canterbury, Christchurch 8041, New Zealand

[2] GEOKEM, P.O. Box 30-125, Barrington, Christchurch, New Zealand

jasonchen1212@hotmail.com

Keywords: *Colloidal silica, nucleation and growth, silica chemistry, Ostwald ripening.*

ABSTRACT

When cooled geothermal brine is reinjected, colloidal silica may form, deposit, and eventually block the fluid pathways in the aquifer, reducing injectivity. Models of silica deposition, the formation of colloidal silica, and especially the growth of silica nanoparticles over time, are of value in the prediction of geothermal well lifetime and the effects of brine treatments and workovers. This paper deals with the growth of silica particles in geothermal brines where silica polymerisation is actively occurring.

Based on the chronomal (Nielsen 1964) and the Ostwald ripening models (Lifshitz and Slyozov 1961, Wagner 1961) and the observations reported by Broge and Iler (1971), Alexander and McWhorter (1976), and Tobler et al. (2009), a semi-empirical silica particle growth model is proposed. It is used to predict silica particle growth over time under typical geothermal conditions, and prepares the groundwork for a model of stability (resistance to aggregation) described in another paper at this conference. The model predictions are compared to the field experiments reported by (Tobler and Benning 2013, Mroczek et al. 2017).

1. INTRODUCTION

Under geothermal conditions, homogeneous nucleation is expected to be the dominant mechanism of initial particle formation (Weres et al. 1981). Molecular deposition of monomeric silica to the particle surface should also be taken into account. Iler (1979) showed that, at pH above 6-7, polymerisation and nucleation happen rapidly as the degree of ionisation is relatively high. Small silica particles of 1-2 nm diameter can form in minutes. It is suggested (Vysotskii and Strazhesko 1974) that there are two fundamental mechanisms of silica particle growth in water after nucleation:

1. Growth due to the precipitation of that silicic acid which is already in the solution, onto nuclei surfaces;

2. Growth of larger particles due to dissolution of smaller particles, i.e. Ostwald Ripening.

At later times, Ostwald ripening and aggregation may be the main mechanisms of particle growth, since the first mechanism becomes slower than the second when the degree of silica supersaturation is reduced by polymerisation.

An in-situ particle size measurement experiment (Tobler et al. 2009, Tobler and Benning 2013) showed that the size of colloidal silica particles appearing at the beginning is very close to the critical nucleation size and rapidly grows, then the growth rate reduces, and eventually the particles may converge to a certain definite size. It was suggested (Iler 1979) that the particle growth mechanisms are independent of the concentration of silica when the $SiO_2 : Na_2O$ ratio is a constant (no other salt present), and the final size is dependent on temperature. This conclusion was supported by the observations reported by Alexander and McWhorter (1976) and Broge and Iler (1971), who studied silica particle growth in aqueous solutions at high temperatures and superatmospheric pressures. It was observed that the final particle size increases with rising temperature when the $SiO_2 : Na_2O$ ratio is fixed. Further investigations by Iler (1979) showed the effect of temperature on final silica particle size even more clearly.

It is clear from the above mentioned studies that when the $SiO_2 : Na_2O$ ratio is fixed, final particle size rises with temperature, at least when the ratio is in the range 64 – 470 as used in those studies. However, under typical geothermal conditions, the ratio can be significantly lower than 64. For instance, for an ideal injectate dissolved with 1000 ppm silica and 0.09 M sodium chloride only, the $SiO_2 : Na_2O$ ratio is about 0.37.

If the finding that final particle size is determined by temperature still holds to be true under geothermal conditions, it would be of interest in the present study as it is reasonable to assume the ratio in the injectate is fixed: if the temperature of the injectate is lowered by cooling before reinjection, smaller particles may form, which are expected to be more stable than the larger particles generated in higher temperatures under same chemical conditions, due to the lower attractive potential for the smaller particles.

Although one cannot simply predict that the deposition rate will be decreased due to the higher stability of the smaller particles, as their number concentration will be higher, there may be a noticeable difference in morphology of the silica scale.

More recently, in-situ and time-resolved observations of silica particle growth were made by Tobler et al. (2009; 2013). At room temperature, to trigger the formation of silica particles, acid was added to the solutions of 640 or 1600 ppm silica and 0.02, 0.05, 0.11, or 0.22 M sodium chloride to adjust pH from 12 to neutral in (i.e. pH-induced growth) Tobler et al. (2009); rapid cooling of the solutions of 640 or 960 ppm silica and 0.03 or 0.06 M sodium chloride from 230 ℃ to 30 – 60 ℃ (i.e. temperature induced growth) was used to trigger particle formation in Tobler and Benning (2013),. Both of the experiments were monitored using synchrotron-based small angle X-ray scattering (SAXS) and dynamic light scattering (DLS) systems. After comparing with both the pH-induced and T-induced experiments, Tobler and Benning (2013) concluded that the final particle size depends on temperature but may not depend on concentration of silica, nor on ionic strength, nor on the

methods that induce the silica particle formation, but the induction time and the growth rate may depend on these parameters.

2. KINETICS OF PARTICLE GROWTH

Nielsen (1964) proposed three mechanisms to describe the processes of colloidal particle growth after nucleation: diffusion controlled, mononuclear, and polynuclear growth.

For diffusion limited spherical particle growth, Nielson (1964) suggested that the growth rate can be expressed by:

$$\frac{dR}{dt} = \frac{D(c_b - c_s)\bar{v}_n}{R} \tag{1}$$

where R is the radius of the particle, t is time; for the precipitating species, D is its diffusion coefficient, c_b is its concentration in the bulk solution at time t, c_s is its concentration on the particle surface, and $\bar{v}_n$ is its molar volume, which is about 0.027 m^3 per 1000 mol for amorphous silica (Rumble and CHEMnetBASE 2017). Since the particle surface is recognised as the interphase boundary, it is reasonable to assume that, for the diffusion-controlled mechanism, c_s is equal to the solubility of the precipitating material c_e. Then, Eq. 1 becomes:

$$\frac{dR}{dt} = \frac{D(c_b - c_e)\bar{v}_n}{R} \tag{2}$$

For surface controlled spherical particle growth (the diffusion is relatively rapid when compared to the surface reaction rate, i.e. $c_b \approx c_s$), two mechanisms are involved: mononuclear and polynuclear. Mononuclear growth physically represents the mechanism of a layer-by-layer precipitating process, i.e. a subsequent layer begins to form only when the formation of its previous layer is complete. The growth rate following the mononuclear growth mechanism can be described by:

$$\frac{dR}{dt} = k_m c_b^m R^2 \tag{3}$$

where, for the mononuclear surface reaction, k_m is its rate constant, and m is its reaction order.

Whereas, for polynuclear growth, the subsequent layer can start to grow before the growth of the previous layer is completed. The growth rate dominated by the polynuclear growth mechanism can be defined by:

$$\frac{dR}{dt} = k_p c_b^p \tag{4}$$

where, for the polynuclear surface reaction, k_p is its surface reaction rate constant, and p is its reaction order.

Williams et al. (1985) suggested that all these three mechanisms may be involved in the growth of colloidal particles. For the initially formed nucleus, mononuclear growth may be important; polynuclear growth could be dominant when the nanoparticles grow bigger; in the later stage, diffusion limited growth should be critical. In practice, the mononuclear growth mechanism is usually not considered as it is expected to have effects only in the very early stage (Nishimori et al. 1996).

2.1 Chronomal model

As suggested by (Nishimori et al. 1996), the present work will only consider two particle growth mechanisms that may have significant effects on the silica particle growth after nucleation: polynuclear and diffusion-controlled. To identify which of the two mechanisms dominates, Nielsen's chronomal analysis (Nielsen 1964) can be used.

The reaction degree α is defined by the amount of a certain species reacting at time t, over the total quantity of the species that can participate in the reaction:

$$\alpha = \frac{c_0 - c_b}{c_0 - c_e} \tag{5}$$

where c_0 is the initial concentration of the precipitating species.

A good approximation was proposed by Nielson (1964) to correlate the reaction degree α and the particle radius R at time t:

$$\alpha = \left(\frac{R}{R_e}\right)^3 \tag{6}$$

where R_e is the final particle radius.

For the diffusion-controlled mechanism, by combining Eq. 2, 5 and 6, the time t can be described using the chronomal I_d:

$$t = \frac{R_e^2}{3\bar{v}_n(c_0 - c_e)} I_d \tag{7}$$

And the chronomal I_d, which may be physically understood as a dimensionless time, is defined by:

$$I_d = \int_0^\alpha x^{-\frac{1}{3}} (1 - x)^{-1}\, dx \tag{8}$$

The chronomal I_d can be solved using standard methods (LaMer and Dinegar, 1950):

$$I_d = \frac{1}{2}\ln\frac{1-\alpha}{(1-\alpha^{1/3})^3} - \sqrt{3}\tan^{-1}\frac{\sqrt{3}}{1+2\alpha^{-1/3}} \tag{9}$$

Similarly, for the polynuclear mechanisms, the time t can be expressed using the corresponding chronomal I_p:

$$t = \frac{R_e}{3\bar{v}_n c_0^p k_p} I_p \tag{10}$$

And the chronomal I_p is defined by:

$$I_p = \int_0^a x^{-\frac{2}{3}} (1 - x)^{-p}\, dx \tag{11}$$

Although the solution to Eq. 11 may not be as easy to express explicitly as in Eq. 9, it can be found numerically.

To identify whether the particle growth after the nucleation is fully diffusion limited, one can use Eq. 7 to predict the degree of reaction α over time, and then compare it with experimental observations. Similarly, by substituting experimental results, i.e. the particle size, or the degree of reaction, as a function of time, into Eq. 10 and 11, one may obtain a set of fitted parameters: the reaction rate constant k_p and the reaction order p. By considering the fitted values in the light of the physics of the known growth mechanisms, one can conclude whether the particle growth is following the surface reaction-controlled or the diffusion-controlled mechanism.

2.2 JMAK model

Alternatively, the Johnson-Mehl-Avrami-Kolmogorov (JMAK) theory (Avrami 1939) may be used to model the phase transformation as well. It is based on the following assumptions: (1) the nucleation process is macroscopically homogenous but microscopically random, (2) the growth rate is independent of the fraction of phase transformation (i.e. what proportion of the material has experienced a phase transformation), and (3) the growth is isotropic, i.e. growing in all directions at the same rate. The Avrami equation (Avrami 1939) was derived to describe the fraction of transformed species α:

$$\alpha = 1 - \exp[-k_a(t - t_0)^n] \qquad (12)$$

where k_a is the reaction constant, and the exponent n was suggested by Hulbert to be dependent on the mechanisms of nucleation and growth and the growth dimensionality. For the case of spherical particles formed by the surface reaction-controlled mechanism, n should be equal to 4 for the stage of homogenous nucleation and equal to 3 for the stage of subsequent particle growth (Hulbert 1969).

The Avrami equation can be expressed in logarithmic form:

$$\ln(-\ln[1 - \alpha]) = \ln k_a + n \ln(t - t_0) \qquad (13)$$

If an experimental observation follows the JMAK kinetic model, a straight line should be obtained in a plot of $\ln(-\ln[1 - \alpha])$ over $\ln(t)$, which is conventionally named the Avrami plot.

By assuming that the silica particle growth is limited by surface reaction (i.e. polynuclear growth mechanism), Tobler et al. (2009) fitted their experimental results with both the chronomal and JMAK models, as shown in Table 1.

Based on the fitting results, Tobler et al. (2009 and 2013) concluded that silica particle growth is dominated by the first-order surface reaction and argued that the JMAK model was not valid due to the power component n being far less than 3. Surprisingly, the observed value of n=1.7 is quite close to the reported (Aubert and Cannell 1986) mass fractal dimension D_f for reaction-limited (RL) silica aggregations induced by adding salts, which was estimated to be 1.75 ± 0.05. This was not mentioned by Tobler et al. However, they did analyse the particle shapes, and confirmed that the silica nanoparticles formed did indeed have fractal structures, especially in the early stage. The estimated mass fractal dimension was reported to be a function of time, increasing from ~1 to 2.3-2.4.

Iler (1979), Perry and Keeling-Tucker (2000), and Tobler et al. (2009) all concluded that laboratory-grown amorphous silica colloids have hydrous (i.e. not all inner silica chains completely polymerised to crosslink particles) or porous structures. Naturally formed silica colloids under geothermal conditions may have fractal geometries as well. Therefore, unless it is specified otherwise, the author will only consider the hydrodynamic radius (the radius of an equivalent hard sphere having the same mass diffusivity, which can be measured using dynamic light scattering) or diameter and its subsequent effects in the coming sections.

According to Table 1, apart from the observed induction time, there is a large discrepancy between two of Tobler et al.'s data points with respect to the surface reaction rate k_p between temperature and pH induced experiments under similar conditions (marked in bold). Tobler et al. (2009) suggested that this may be caused by the time needed to reach a certain degree of supersaturation (instantaneous vs. 2-3 minutes).

2.3 Particle growth in the late stages

It is widely accepted that Ostwald ripening (OR) is one of the crucial mechanisms in the late stages of silica particle growth (Iler 1979, Perry and Keeling-Tucker 2000, Tobler et al. 2009, Tobler and Benning 2013).

Although the phenomenon of Ostwald Ripening was discovered and described in 1896 by Wilhelm Ostwald, it was not successfully modelled until 1958 by Lifshitz and Slyozov, and 1961 by Wagner, who independently concluded the same results by adopting different approaches. Combined, these works are known as the Lifshitz-Slyozov-Wagner (LSW) theory of Ostwald Ripening.

When the diffusion of the monomers limits the particle growth, the average particle size $\bar{R}$ can be estimated using (Lifshitz and Slyozov 1961):

$$\bar{R}^3 = \frac{4}{9} D \alpha_{OR} \nu t \qquad (14)$$

Table 1: Summary of the obtained parameters by postprocessing the experimental results, reproduced from (Tobler et al. 2009): the initial particle growth rate G_0 and the reaction constant k_p were fitted with the chronomal model; the estimated radius of nuclei R_0^+ and R_0 was respectively obtained by using the theoretical expression Eq. 20 below (assuming the surface tension is fixed at 0.078 ± 0.0034 J m^{-2}) and extrapolating the fitted chronomal model curve to $t = 0$; the reaction constant k_a was fitted with the JMAK model.

Method	Initial [SiO_2] (ppm)	Induction time (min)	Ionic strength (M)	R_0^+ (nm)	Chronomal Analysis				JMAK model		Aggregation observed (by DLS)?
					R_0 (nm)	G_0 (10^{-3} s^{-1})	k_p (10^{-4} s^{-1})	p	k_a (10^{-4} s^{-1})	n (averaged)	
pH induced (adjusting pH from 12 to 7)	**640**	**< 10**	**0.02**	**1.07**	**1.09**	**0.70**	**5.13**	**1**	**2.77**	**1.7 ± 0.1**	**No**
		< 10	0.11	1.06	1.00	1.09	7.75	1	3.34	1.7 ± 0.1	No
		< 10	0.22	1.04	1.05	1.20	8.22	1	3.61	1.7 ± 0.1	No
	1600	< 10	0.05	0.68	-	-	-	-	-	-	No
		< 10	0.22	0.67	-	-	-	-	-	-	Yes, at t = 30 min
T induced (rapid cooling from 230 ℃ to 30-60 ℃)	**640**	**~60**	**0.06**	**1.07**	**-**	**-**	**<1.46**	**1**	**-**	**-**	**No**
	960	< 10	0.03	0.85	1.47	-	1.46	1	-	-	No

where D is the diffusion coefficient of the monomers, t is time since Ostwald Ripening begins, and the parameter α_{OR} is a function of surface tension γ, temperature T, and the solubility of the monomers C_∞:

$$\alpha_{OR} = \frac{2\gamma\nu C_\infty}{R_g T} \quad (15)$$

where the constants ν and R_g are the molar volume of the precipitating material and the ideal gas constant, respectively.

More conveniently, if particle growth follows the model derived by Lifshitz and Slyozov (1961), under certain conditions, one will observe the average particle size increase as a function of $t^{1/3}$, i.e.

$$\bar{R} \propto t^{1/3} \quad (16)$$

When the surface reaction (i.e. the precipitation of monomers, assumed to be a first order reaction) dominates the particle growth, the average particle size $\bar{R}$ may be predicted using:

$$\bar{R}^2 = \frac{32}{81}\alpha_{OR} k_s \nu t \quad (17)$$

where k_s is the net precipitation rate of monomers.

If particle growth follows the model shown in Eq. 17, one would see the average particle size increase as a function of $t^{1/2}$, i.e.

$$\bar{R} \propto t^{1/2} \quad (18)$$

Depending whether the particle growth obeys either Eq. 16 or Eq. 18, one could easily determine whether the sol development is dominated by Ostwald Ripening or whether other mechanisms should be considered. After fitting their pH induced observations with the LSW theory, Tobler et al. (2009) concluded that Ostwald ripening may dominate the silica particle growth only in the late stages, and the Ostwald ripening mechanism is not valid to model the entire silica particle growth process.

In their later investigations (Tobler and Benning 2013), i.e. the temperature induced experiments, it was claimed that any attempt for fitting the observations with Ostwald ripening model may be impractical due to the particle growth being incompletely recorded, i.e. experiments were stopped once the final particle size was reached. To further study the problem, the experimental results were replotted and independently fitted by the present author as shown in Fig. 1 below:

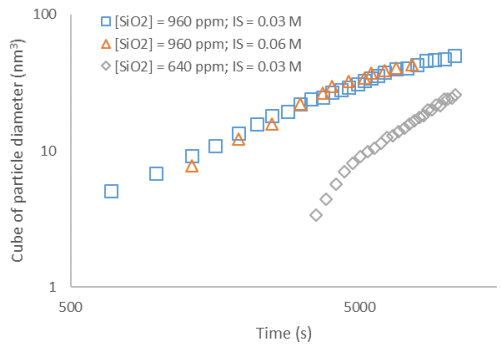

(a)

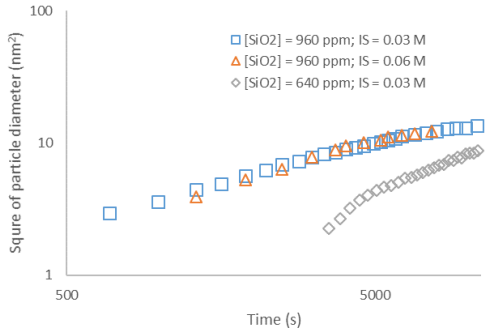

(b)

Figure 1: (a) Cube of particle radius and (b) square of particle radius over time. Observations are reproduced from (Tobler and Benning 2013).

Compared to the fitting results shown in (Tobler et al. 2009), these two sets are a better fit to a linear function. This suggested to the author that Ostwald ripening may not be valid for describing the whole particle growth process but could have a $t^{1/3}$ period and a $t^{1/2}$ period that can be fitted with the Ostwald Ripening model separately.

3. HYPOTHESIS

We propose that, leaving aside aggregation for the moment and assuming that the nucleation process is instantaneous, homogenous silica nucleation and the subsequent particle growth can be modelled as a three-stage process, as shown in Fig. 2 Below.

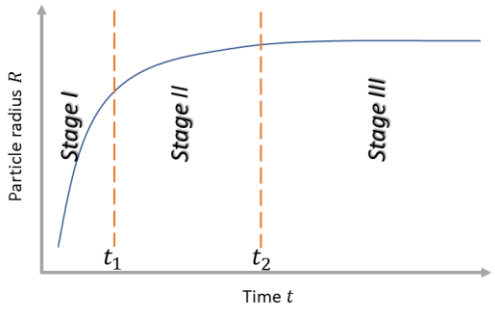

Figure 2: Qualitative plot of three-stage particle growth, where t_1 and t_2 represent the end of Stage I and II respectively.

1. Stage I: initial surface reaction-controlled particle growth

The first stage may be rapid as the degree of supersaturation (quantitatively described by the silica supersaturation index, SSI) is relatively large in the early stage. When the concentration of dissolved silica along with silica saturation index SSI drops due to the formation of silica particles, the particle growth rate dR/dt decreases and the diffusion-controlled mechanism becomes more important.

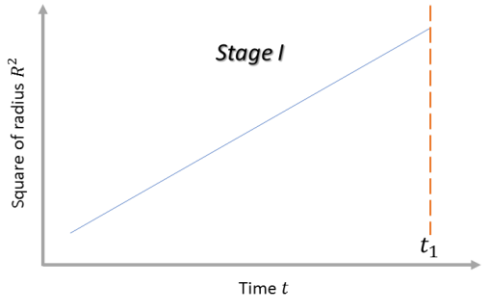

Figure 3: Qualitative plot of Stage I: initial particle growth

Hence, in Stage I, the square of average silica particle radius $\bar{R}^2$ is proportional to the time t, i.e.:

$$\bar{R}^2 = k_1 t + b_1 \quad \text{for} \quad t < t_1 \tag{19}$$

Since Stage I is proposed to be a surface reaction-controlled process, similar to the precipitation rate of monomeric silica determined by temperature, pH, ionic strength, and the degree of silica supersaturation, the slope k_1 is expected to depend on all these factors as well.

Theoretically, the intercept b_1 should not be less than square of the initial critical nucleation radius (i.e. $b_1 \geq R_{crit,0}^2$ to reasonably predict the particle size at the beginning of the whole process (i.e. $t = 0$). $R_{crit,0}$ can be found using the Gibbs-Kelvin equation (Gibbs 1961):

$$R_{crit,0} = \frac{2\gamma}{\rho_N k_B T \ln \mathrm{SSI}} \tag{20}$$

where γ is the interfacial free energy, ρ_N is the number density of SiO_2 units in solid amorphous silica, T is the absolute temperature, and SSI is the silica supersaturation index (the ratio of the concentration of dissolved silica to the solubility of amorphous silica). For simplicity, it may be reasonable to let $b_1 = R_{crit,0}$.

This stage ends when the final particle size $R_{max,1}$ is reached at t_1.

2. Stage II: subsequent growth due to diffusion-controlled Ostwald ripening until the surface silica concentration reaches equilibrium, i.e. $dR/dt = 0$ due to $c_b = c_e$.

In the second stage, the diffusion-controlled mechanism becomes dominant. This stage may last longer than Stage I, and has slower particle growth than the previous stage. It ends when the equilibrium is reached (i.e. the particle stops growing and becomes stable). Based on the observations reported by (Tobler et al. 2009, Tobler and Benning 2013, Mroczek et al. 2017), when the equilibrium mentioned above is reached, it may not be necessary for SSI to be equal to one.

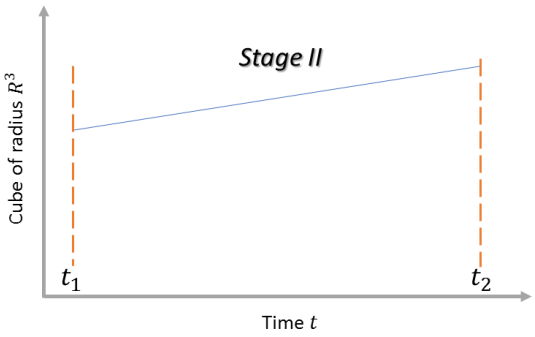

Figure 4: Qualitative plot of Stage II: subsequent particle growth

Hence, in stage II, the cube of average silica particle radius $\bar{R}^3$ is proportional to the time t, i.e.:

$$\bar{R}^3 = k_2(t - t_1) + b_2 \quad \text{for} \quad t_1 \leq t < t_2 \tag{21}$$

As Stage II is considered to be a diffusion-limited process, the slope k_2 is expected to be mainly dependent on temperature, and pH, ionic strength, and the degree of silica supersaturation may play roles as well.

b_2 shall be equal to cube of the particle size at $t = t_1$, which is the maximum particle size in Stage I:

$$b_2 = R_{max,1}^3 \quad \text{when} \quad t = t_1 \tag{22}$$

This stage ends when the final particle size R_{max} is reached at t_2.

3. Stage III: steady state where particles stop growing

If the conditions do not favour aggregation, silica particles suspended in water can exist for years or even decades without noticeable variation in size (Iler 1979).

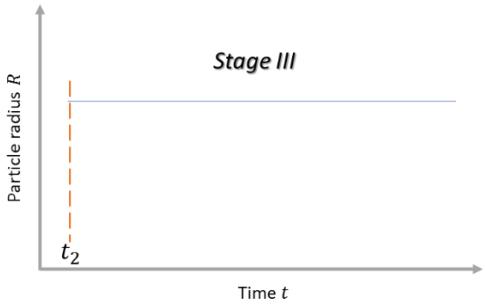

Figure 5: Qualitative plot of Stage III: steady state

Hence, in stage III, if temperature is constant, the average particle size is expected to be fixed at the final size R_{max}, i.e.:

$$\bar{R} = R_{max} \quad \text{for} \quad t \geq t_2 \tag{23}$$

4. FITTING RESULTS AND DISCUSSION

4.1 Results

Since there are few time-resolved silica particle growth observations where silica polymerisation is actively happening, only the experimental results reported by (Tobler et al. 2009) are used to find k_1, $R_{max,1}$(i.e. $b_2^{1/3}$) for Stage I

and k_2 for Stage II. The observations in (Tobler and Benning 2013) are used for validation.

As shown in Fig. 1, a critical time t_1 separates Stage I and II. After the maximum particle size in Stage I $R_{max,1}$ is reached at t_1, one can observe an obvious change in slope that marks the end of Stage I, as shown in Fig. 6 below.

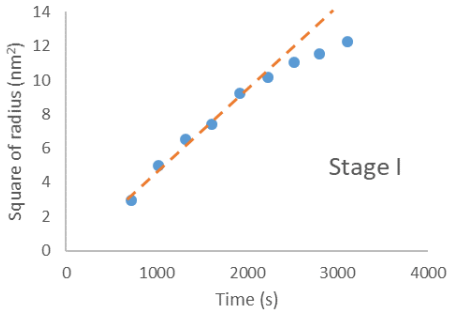

Figure 6: Square of particle radius over time, fitted with a linear correlation (dash line). The observations (dots) are reproduced from (Tobler et al. 2009): the pH-induced experiment in the 0.22 M ionic strength solution initially dissolved with 640 ppm monomeric silica at pH = 12 and room temperature. Note that the last three points are offset from the fitted line.

Therefore, the first point that has the obvious offset is recognised as the maximum particle size in Stage I $R_{max,1}$. According to all available particle growth history data, it is found that the ratio of $R_{max,1}$ to the final particle size R_{max} (i.e. $R_{max,1}/R_{max}$) is about 0.80. Therefore, for simplicity, $R_{max,1}$ is empirically defined by:

$$R_{max,1} = 0.80\, R_{max} \qquad (24)$$

The experiment in (Tobler et al. 2009) was done at 25℃, neutral pH, ionic strength (I) 0.02, 0.05, 0.11, 0.22 M, and SSI ~5.46 and ~13.64. By plotting the candidate points (i.e. observed particle size history) on axes of time and radius squared or cubed (for Stage I and II respectively) as in Fig. 6, one can easily find the slope $k_1$and k_2 for Eq. 19 and 21 separately.

For each experiment under certain conditions (ionic strength and SSI), there is a pair of $k_1$and k_2 (six pairs under six sets of conditions in total). By treating the two conditions as free parameters, the following correlations can be fitted:

for $0 \leq t < t_1$ (i.e. Stage I)

$$k_1 = 0.0019 + 9.2\times10^{-5}\mathrm{SSI} + 0.020I - 7.0\times10^{-4}\mathrm{SSI}\cdot I - 0.033I^2 \qquad (25)$$

for $t \geq t_2$ (i.e. Stage II)

$$k_2 = -3.5\times10^{-4} + 9.6\times10^{-4}\mathrm{SSI} + 0.026I - 0.0048\mathrm{SSI}\cdot I - 0.031I^2 \qquad (26)$$

R^2 (the coefficient of determination, indicating the viability of the fitted function) for Eq. 25 and 26 are > 0.99.

The reported final particle sizes (Alexander and McWhorter 1976; Broge and Iler 1971; Tobler et al. 2009; Tobler and Benning 2013) can be plotted in Fig. 7 below:

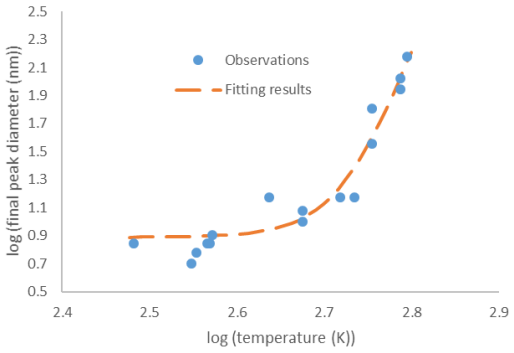

Figure 7: Reported final particle diameter as a function of temperature in a logarithmic scale.

These observations were reported under the conditions of SiO_2: Na_2O mole ratio from very high (due to very low salt concentration) to about 0.1, SSI from about 163 to 5.46, ionic strength from 0.22 to very low, pH around neutral, and temperature from room temperature to 350 ℃.

It can be seen that the final particle size is sensitive principally to temperature, increasing exponentially, and is much less sensitive to other parameters. Thus, the final silica particle diameter D_{max} in the temperature range from 298 to 623 K (i.e. $25-350$ ℃) may be empirically expressed by:

$$D_{max} = 1.7\times10^{-5}\exp(0.025T) + 7.7 \qquad (27)$$

where D_{max} is in nm. The R^2 for Eq. 27 is > 0.90. The predictions made from Eq. 27 are plotted as the orange dashed curve in Fig. 7.

4.2 Extrapolation

Since the temperature and SSI of the available data lie outside typical geothermal conditions (e.g. in the case of geothermal reinjection in New Zealand fields: T = ~160 ℃, I = ~0.09 M, SSI = ~1.5, and pH close to neutral if not acidified), extrapolations have to be made.

In Stage I, the surface reaction limits the silica particle growth. Based on the LSW theory and the proposed three-stage silica particle growth model (Eq. 17 and 19), k_1 is seen to be proportional to $\frac{64}{81}\frac{\gamma v C_\infty}{R_g T}k_s$.

As the temperature T varies, the surface tension γ can be predicted by following (Weres et al. 1980); the solubility C_∞ change is well-known (Iler 1979, Gunnarsson and Arnórsson 2000); k_s is essentially the rate of the reaction between silicic acid and amorphous silica surfaces. (Fleming 1986) suggested that this reaction showed an Arrhenius temperature dependence with an activation energy of 13.1 ± 0.9 kcal mol^{-1}in the temperature range of $25-100$ ℃. We assume this relationship can be extrapolated to typical geothermal conditions. Hence, k_s can be represented by:

$$k_s = k_s^{298K}\exp\left[-\frac{E}{R_g}\left(\frac{1}{T}-\frac{1}{298.15}\right)\right] \qquad (28)$$

where k_s^{298K} is the reaction rate at 298 K, and E is the activation energy.

Therefore, k_1 can be re-expressed by:

$$k_1 = \frac{\gamma C_\infty}{T} \frac{298.15}{\gamma^{298K} C_\infty^{298K}} \frac{k_s}{k_s^{298K}} k_1^{298K} \quad (29)$$

where γ^{298K} and C_∞^{298K} are the surface tension and the solubility at 298 K, and k_1^{298K} is equivalent to k_1 predicted in Eq.23.

By combining Eq. 28 and 29:

$$k_1 = \frac{\gamma C_\infty}{T} \frac{298.15}{\gamma^{298K} C_\infty^{298K}} \exp\left[-\frac{E}{R_g}\left(\frac{1}{T} - \frac{1}{298.15}\right)\right] k_1^{298K} \quad (30)$$

The SSI in the data used is also out of the range of typical geothermal conditions. However, the coefficients preceding SSI in Eq. 25 are quite small compared to those of ionic strength, suggesting that the effects of SSI on k_1 are limited. Therefore, it may be safely assumed that Eq. 25 and 30 can be used in a wider SSI range than $\sim 5.46 - \sim 13.64$ as the introduced errors may only have very limited effects on k_1.

In stage II, the diffusion of monomeric silica limits the silica particle growth. According to the LSW theory and the proposed three-stage silica particle growth model (Eq. 14 and 21), k_1 may be reasonably considered to be proportional to $\frac{4}{9} D \frac{\gamma v C_\infty}{R_g T} v$.

Given that temperature is changing, the diffusion coefficient for monomeric silica D may be calculated from the Einstein-Stokes equation (Rebreanu et al., 2008):

$$D = \frac{k_B T}{6\pi\mu r} \quad (31)$$

where μ is the dynamic viscosity of the solution, and r is the radius of silicic acid molecule. Since $k_B/6\pi r$ is independent of temperature, D is proportional to T/μ. By assuming the dynamic viscosity of the solution is equal to that of water at the same temperature, μ as a function of temperature can be easily found in (Keenan 1978). Other parameters, such as γ, C_∞, and SSI, are handled similarly.

Therefore, k_2 can re-expressed by:

$$k_2 = \frac{T}{\mu} \frac{\gamma C_\infty}{T} \frac{\mu^{298K}}{298.15} \frac{298.15}{\gamma^{298K} C_\infty^{298K}} k_2^{298K} \quad (32)$$

where k_2^{298K} is equivalent to k_2 predicted in Eq.26.

By rearranging:

$$k_2 = \frac{\gamma C_\infty}{\mu} \frac{\mu^{298K}}{\gamma^{298K} C_\infty^{298K}} k_2^{298K} \quad (33)$$

4.3 Validation

To validate the performance of the model, two examples are used: one is the pH-induced observations in (Tobler et al. 2009) at 25℃, neutral pH, I = 0.22 M, and SSI = ~5.46, the other is the T-induced experimental results from (Tobler and Benning 2013) at 30℃, neutral pH, I = 0.06 M, and SSI = ~5.46.

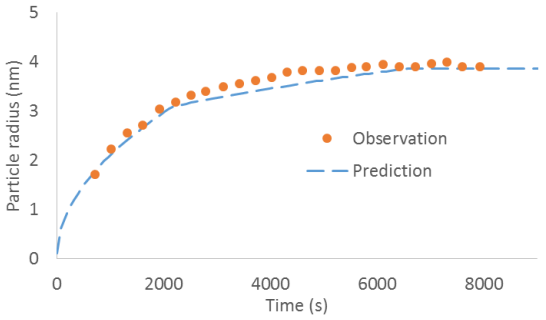

(a)

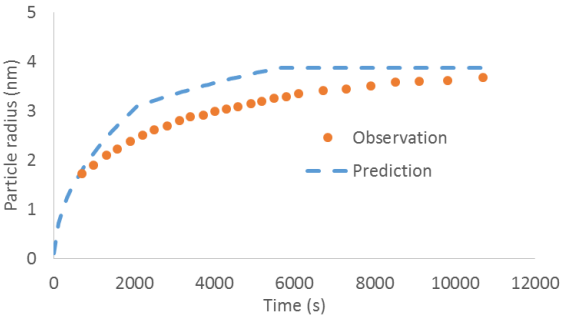

(b)

Figure 8: Comparison between observations and predictions at (a) 25℃, neutral pH, I = 0.22 M, and SSI = ~5.46 and (b) 30℃, neutral pH, I = 0.06 M, and SSI = ~5.46; observations reproduced from (Tobler et al. 2009; Tobler and Benning 2013).

It can be seen that the three-stage particle growth model can reasonably predict the silica particle size as a function of time if the polymerisation is pH induced, but a discrepancy exists when the polymerisation is temperature induced. Tobler and Benning (2013) considered this as the consequence of the supersaturation differences at the early stage. In the pH-induced experiment (Tobler et al. 2009), the supersaturation is established within 30 s by adjusting pH from 12 to 7 (i.e. a sudden SSI jump); in the temperature-induced experiment (Tobler and Benning 2013), the supersaturation is reached by cooling the solution from 230 to 30 ℃ in about 3 min (i.e. a gradual SSI increase). Therefore, the discrepancy suggests that the model is more suitable to predict the silica particle growth in conditions where the silica polymerisation is triggered instantaneously.

On the other hand, one may note that, despite the discrepancy at the early stage, good agreement is obtained for the final particle size R_{max}. Mroczek et al. (2017) reported a field observation that silica nanoparticles with an average diameter of 8-9 nm at about 80 ℃. By following Eq. 27, it is predicted that the final particle size D_{max} is about 7.8 nm under the same conditions. This suggests the model is able to predict the final silica particle size some geothermal brines.

5. CONCLUSION

A concept for a three-stage silica particle growth model has been proposed. Key parameters (k_1, k_2, $R_{max,1}$, R_{max}) have been fitted to the data of (Broge and Iler 1971; Alexander and McWhorter 1976; Tobler et al. 2009). The predictions of

particle size history reasonably match observations for pH-induced silica particle growth (Tobler et al. 2009), however the agreement is less satisfactory for the T-induced silica particle formation (Tobler and Benning 2013). Final particle size prediction is equally good for both pH and T-induced experiments, and also for the field observations of (Mroczek et al. 2017).

Further investigations on the time-resolved silica particle growth in a wider range of pH, temperature, ionic strength, and initial concentration of the dissolved silica may be of interest.

REFERENCES

Alexander, G. B., and J. R. McWhorter (1958). U.S. Pat. 2.833,724 (Du Pont).

Aubert, C. and D. S. Cannell (1986). "Restructuring of colloidal silica aggregates." Physical review letters **56**(7): 738-741.

Avrami, M. (1939). Kinetics of phase change. I General theory. The Journal of chemical physics, **7**(12), 1103-1112.

Broge, E. C., and R. K. Iler (1954) U.S. Pat. 2,680,721 (Du Pont).

Fleming, B. A. (1986). "Kinetics of reaction between silicic acid and amorphous silica surfaces in NaCl solutions." Journal of Colloid and Interface Science **110**(1): 40-64.

Gibbs, J. W. (1961). The scientific papers of JW Gibbs, vol. 1.

Gunnarsson, I. and S. Arnórsson (2000). "Amorphous silica solubility and the thermodynamic properties of H4SiO4 in the range of 0° to 350°C at Psat." Geochimica et cosmochimica acta **64**(13): 2295-2307.

Hulbert, S. F., (1969) "Models for Solid-State Reactions in Powdered Compacts: A Review." The Journal of the British ceramic society, **6**(1), 11-20.

Iler, R. K. (1979). "Chemistry of Silica--Solubility, Polymerization, Colloid and Surface Properties, and Biochemistry."

Keenan, J. H. (1978). Steam tables: thermodynamic properties of water including vapour, liquid, and solid phases (International system of units - S.I.). N.Y, Wiley.

Lifshitz, I. M. and V. V. Slyozov (1961). "The kinetics of precipitation from supersaturated solid solutions." Journal of physics and chemistry of solids **19**(1-2): 35-50.

Mroczek, E., et al. (2017). "Silica scaling in cooled silica saturated geothermal water: Comparison between Wairakei and Ohaaki geothermal fields, New Zealand." Geothermics **69**: 145-152.

Nielsen, A. E. (1964). Kinetics of precipitation, Pergamon.

Nishimori, H., Tatsumisago, M., and Minami, T. (1997). Growth mechanism of large monodispersed silica particles prepared from tetraethoxysilane in the presence of sodium dodecyl sulfate. Journal of Sol-Gel Science and Technology, **9**(1), 25-31.

Perry, C. C. and T. Keeling-Tucker (2000). "Model studies of the precipitation of silica in the presence of aluminium; implications for biology and industry." Journal of Inorganic Biochemistry **78**(4): 331-339.

Rumble, J. and CHEMnetBASE (2017). CRC Handbook of Chemistry and Physics, 98th Edition. Boca Raton Florence, CRC Press LLC Taylor & Francis Group Distributor**:** 1 online resource.

Tobler, D. J. and L. G. Benning (2013). "In situ and time resolved nucleation and growth of silica nanoparticles forming under simulated geothermal conditions." Geochimica et cosmochimica acta **114**: 156-168.

Tobler, D. J., et al. (2009). "Quantification of initial steps of nucleation and growth of silica nanoparticles: An in-situ SAXS and DLS study." Geochimica et cosmochimica acta **73**(18): 5377-5393.

Vysotskii, Z. and D. Strazhesko (1974). The role of polymerization and depolymerization reactions of silicic acid, etc, Wiley New York**:** pp. 55-75.

Wagner, C. (1961). "Ostwald ripening theory." Ber. Bunsenges. Phys. Chem **65**: 581-591.

Williams, R., Yocom, P. N., and Stofko, F. S. (1985). Preparation and properties of spherical zinc sulfide particles. Journal of colloid and interface science, **106**(2), 388-398.

Weres, O., et al. (1981). "Kinetics of silica polymerization." Journal of Colloid and Interface Science **84**(2): 379-402.